Full Length Article

JHS(E)

Journal of Hand Surgery
(European Volume)
2019, Vol. 44(10) 1056–1064

DOI: 10.1177/1753193419866598
journals.sagepub.com/home/jhs


Carpal kinematic changes after scaphoid nonunion: an in vivo study with four-dimensional CT imaging

Marieke G. A. de Roo[1,2], Johannes G. G. Dobbe[2], Chantal M. A. M. van der Horst[1], Geert J. Streekstra[2] and Simon D. Strackee[1]

Abstract

The aim was to evaluate if motion between the scaphoid bone fragments is related to the position of the fracture line and if a scaphoid nonunion results in the uncoupling of the proximal and distal carpal row during wrist motion. The influence of dorsal intercalated segment instability on interfragmentary motion was also analysed. In this study, 12 patients were included with unilateral scaphoid nonunion. Four-dimensional computerized tomography was used to analyse flexion–extension and radioulnar deviation motion of both wrists. We found that an increased instability of the scaphoid fragments is associated with the presence of dorsal intercalated segment instability and is not dependent on the position of the fracture line relative to the scaphoid apex. Additionally, a scaphoid nonunion results in an uncoupling of the carpal rows.

Keywords

Scaphoid nonunion, dynamic imaging, 4-D-CT imaging, scaphoid fracture, wrist kinematics, in-vivo kinematics, dynamic imaging, 4-D imaging, 3-D motion analysis

Date received: 22nd February 2019; revised: 27th June 2019; accepted: 9th July 2019

Introduction

When healing of a scaphoid fracture fails, the nonunion causes changes in wrist mechanics with severe degeneration of the wrist joint, eventually resulting in a specific pattern of carpal collapse (scaphoid nonunion advanced collapse (SNAC) wrist) (Mack et al., 1984). The speed in which the different stages of a SNAC wrist progress varies between patients (Mack et al., 1984). Currently it is unknown how a scaphoid nonunion precisely influences a carpal collapse and which factors contribute to faster progression of the SNAC stages (Miric et al., 2000). Factors that are considered to be associated with a rapid occurrence of carpal collapse are fracture location (Moritomo et al., 1999, 2000, 2008; Oka et al., 2005; Werner et al., 2016a), humpback deformity (Moritomo et al., 2000), concomitant ligament injuries (Tatebe et al., 2016; Wong et al., 2005) and lunate morphology (Haase et al., 2007; Kim et al., 2016). A few studies have measured in vivo scaphoid nonunion kinematics using static three-dimensional (3-D)-imaging techniques (Leventhal et al., 2008; Moritomo et al., 2008). Moritomo et al. (2008) describe a mobile-type scaphoid nonunion and a stable-type scaphoid nonunion. They found that the amount of interfragmentary motion between the scaphoid fragments predominantly depends on whether the fracture line passes distal or proximal of the scaphoid apex (Figure 1). A distal fracture line would result in an increase of interfragmentary motion. Leventhal et al. (2008) could not associate fracture location to the amount of interfragmentary motion, but did observe an uncoupling of the distal and proximal carpal row after scaphoid nonunion.

[1]Plastic, Reconstructive and Hand Surgery, University of Amsterdam, Amsterdam UMC, AMC, Amsterdam, Netherlands
[2]Biomedical Engineering and Physics, University of Amsterdam, Amsterdam UMC, AMC, Amsterdam, Netherlands

Corresponding Author:
Marieke G. A. de Roo, Plastic, Reconstructive and Hand Surgery, Amsterdam UMC, University of Amsterdam, Amsterdam Movement Sciences, Meibergdreef 9, Amsterdam UMC, AMC, Amsterdam, Netherlands.
Email: m.g.deroo@amc.uva.nl

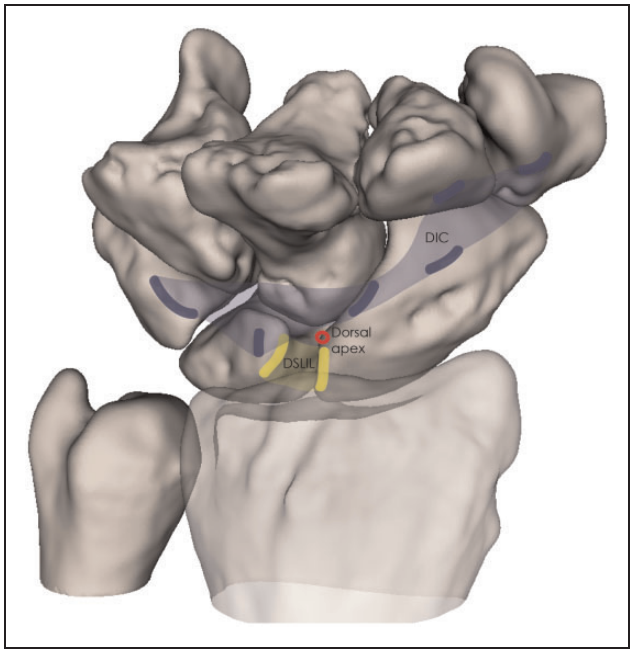

Figure 1. Dorsal view of the carpus demonstrating the location of the dorsal apex of the scaphoid (red circle), and its position in relation to the surrounding ligaments DSLIL (dorsal scapholunate ligament, yellow colour) and the DIC (dorsal intercarpal ligament, blue colour). According to Moritomo et al. (2008) a fracture line proximal to the apex would result in a stable type of scaphoid nonunion, since the dorsal scapholunate ligament would stabilize both scaphoid fragments.

These studies were based on static 3-D views of the carpus in a limited number of wrist positions. However, abrupt displacements or transitory adapted motion patterns that occur during wrist motion may not be shown using static imaging techniques. Dynamic scapholunate dissociation may only be visible with dynamic radiographic imaging (Adolfsson and Povlsen, 2004; Slutsky, 2008). This phenomenon could also be present in scaphoid nonunion wrists, as a high incidence of associated carpal ligament injuries is described (Tatebe et al., 2016; Wong et al., 2005). In four-dimensional (4-D) CT imaging, a series of 3-D images are acquired over time (time being the fourth dimension) to allow detection of motion of the bones in the wrist.

This study analyses the adapted kinematics of the wrist following scaphoid nonunion using in vivo 4-D-CT imaging. The two primary endpoints are: (1) which factors influence the amount of interfragmentary motion between the scaphoid fragments? (2) what is the effect of a scaphoid nonunion on carpal kinematics? For the primary endpoint one, the primary research question was: is motion between the scaphoid bone fragments related to the position of the fracture line with respect to the scaphoid apex? We hypothesize that the scaphoid fragment motion pattern is dependent on the position of the fracture line. The secondary objectives of primary endpoint 1 are to evaluate if other clinical parameters correlate to an increased fragment instability, such as the presence of dorsal intercalated segment instability (DISI) deformity (radiolunate angle $> 15^{\circ}$), duration of nonunion, wrist movement and flexion deformity of the scaphoid nonunion. For primary endpoint two, the research question is: does a scaphoid nonunion result in uncoupling of the proximal and distal carpal row during wrist motion (yielding an adapted motion pattern)? We hypothesize that scaphoid nonunion results in uncoupling of the distal and proximal carpal row.

Methods

Patients

Between March 2016 and October 2018, a prospective multicentre study was carried out in the Amsterdam UMC, location AMC and the OLVG, location Oost, according to the strengthening the reporting of observational studies in epidemiology (STROBE) guidelines (von Elm et al., 2014). Patients were eligible for inclusion if they presented with a unilateral scaphoid nonunion (diagnosis based on a radiograph or CT scan, > 4 months after injury, with the absence of trabecular bridging (described by the radiologist)) (Ferguson et al., 2016), a contralateral wrist with no history of trauma, were 16 or more years of age, and willing and able to give informed consent. Exclusion criteria were a history surgery for the scaphoid nonunion, pregnancy and known skeletal and/or connective tissue diseases. Written information (including radiation dose), personal explanation and brochures were provided. Informed consent was signed before scans were acquired. Thirteen patients (12 men, one woman) were eligible for inclusion. One patient was excluded after scans were obtained, since he appeared not to be able to follow the instructions of the wrist motion protocol. Therefore scans of 12 patients (11 men, one woman; mean age 30 years, range 17 to 46) were included for this trial. Patient characteristics, fracture specifications, distal fragment collapse, lunate type, presence of DISI and carpal degenerative changes are described in Table 1. Data collection was approved by the Medical Ethics Committee (NL56112.018.15) of the Amsterdam UMC, location AMC.

Image acquisition

Each patient was placed in prone position with the arm in a special positioning device to immobilize

Table 1. Patient data.

Case	Age (years)	Duration of nonunion (months)	Fracture line relative to apex	Fracture classification			Distal fragment collapse		Lunate type	Radiolunate angle (degrees)	DISI deformity	Degenerative change
				Herbert	Garcia-Elias	Moritomo	Δ_{tot} (mm)	Φ_{tot} (degrees)				
1	25	14	Proximal	B3	Type 1		1	12	2	14	Absent	Absent
2	46	9	Distal	B2			2	24	1	12	Absent	DRU, RSJ
3	35	11	Distal	B1		Type 2	3	32	1	20	Present	RSJ
4	23	42	Proximal	B1		Type 1	2	33	1	24	Present	RSJ
5	53	5	Distal	B1		Type 2	2	15	1	-5	Absent	Absent
6	17	11	Proximal	B1		Type 1	3	29	1	12	Absent	Absent
7	26	6	Distal	B3	Type 2		4	19	1	11	Absent	Absent
8	21	9	Proximal	B3	Type 1		4	21	2	30	Present	RSJ, STT
9	23	10	Proximal	B3	Type 1		2	18	2	3	Absent	Absent
10	25	9	Proximal	B3	Type 1		1	9	2	5	Absent	Absent
11	37	45	Proximal	B1		Type 1	1	32	1	20	Present	RSJ, STT
12	32	14	Distal	B2			1	37	2	20	Present	RSJ

All patients were men except #7.

Δ_{tot}: total translation of the distal fragment relative to the proximal fragment; Φ_{tot}: total rotation of the distal fragment relative to the proximal fragment; Degenerative change as described by the radiologist on the initial CT scan at presentation; DISI: dorsal intercalated segment instability; DRU: distal radioulnar joint; RSJ: radioscaphoid joint; STT: scaphotrapeziotrapezoidal joint.

the elbow and radius. The patients held a rod that allows motion in the flexion–extension (FE) or radioulnar deviation (RUD) direction of the wrist joint (Figure 2). First a static 3-D-CT scan of the radius and wrist in neutral position (dorsum of the hand and third metacarpal aligned with the forearm) was acquired with a 64-slice Brilliance CT scanner (Philips Healthcare, Cleveland, OH, USA) (120 kV, 75 mAs). Four-dimensional CT scans were obtained during 12 seconds of active wrist motion (120 kV, 30 mAs, collimation 64×0.625 mm, axial field of view 4 cm, rotation time 0.4 s), in which the wrist moved from extension to flexion, and subsequently from radial to ulnar deviation. First the contralateral unharmed wrist was scanned, then the wrist with the scaphoid nonunion within pain limits. In total the patients received a dose of 0.3 mSv.

Image analysis

All scans of the left wrist were mirrored to right wrists to render identical data analysis. The proximal scaphoid fragment, distal scaphoid fragment, lunate, capitate and radius were segmented from the static 3-D-CT scan, resulting in 3-D polygons. These 3-D polygons were matched to the 30 time frames of the 4-D-CT scan. An in-depth explanation of this validated image analysis method is explained by Dobbe et al. (2019). The applied analysis method has a systematical error in estimating kinematic parameters of <1 mm for translational and $<2^{\circ}$ for rotational parameters.

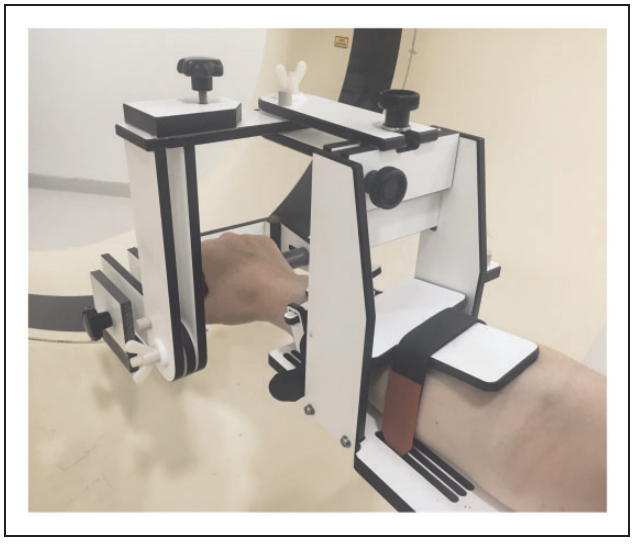

Figure 2. The participant lies in prone position with the hand enclosing a rod. This rod can be repositioned to place the wrist in the centre of rotation. The custom-made positioning device allows active wrist motion along the flexion–extension and radioulnar deviation motion axes.

Describing kinematics

An anatomical coordinate system was automatically determined for each radius (Figure 3) (Vroemen et al., 2012). Wrist flexion ($x+$), extension ($x-$), radial- ($y+$), ulnar deviation ($y-$), supination ($z+$) and pronation ($z-$) were defined as rotation of the capitate around the axes of the radial coordinate system. The capitate was used to express global wrist motion (Citteur et al., 1998; de Lange et al., 1985; Rainbow et al., 2013). The positions of the bones obtained from the 3-D-CT scan of the wrist defined the neutral wrist position.

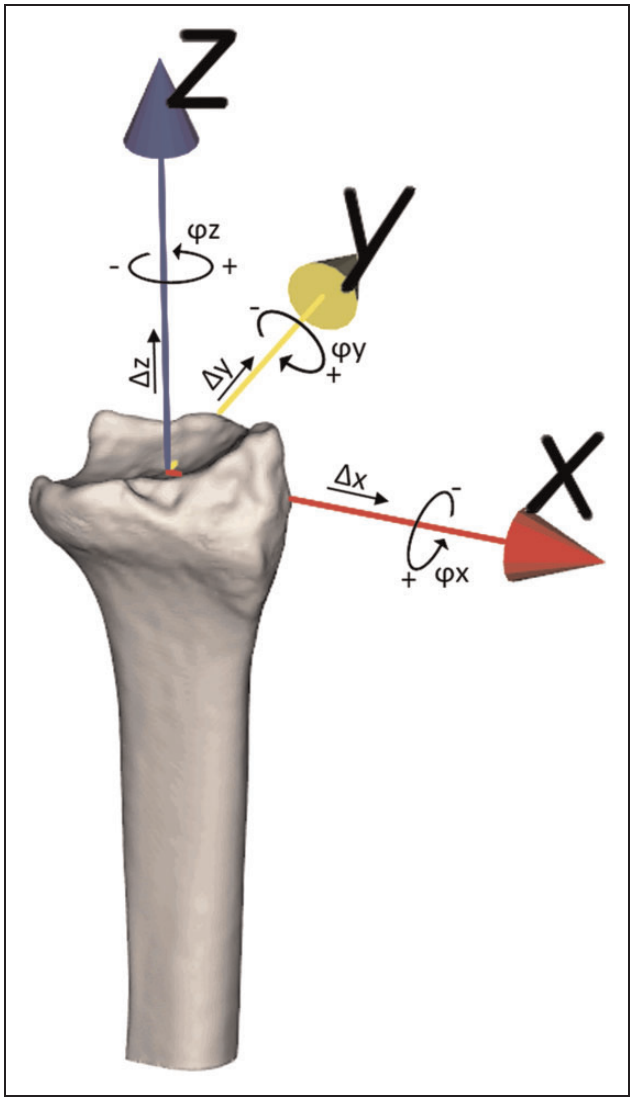

Figure 3. Anatomical coordinate system of the radius. Motion is expressed in terms of translations along the axes (Δx, Δy, Δz) and rotations about the axes (ϕx, ϕy, ϕz), yielding wrist flexion ($\phi x+$), extension ($\phi x-$), radial- ($\phi y+$), ulnar deviation ($\phi y-$), supination ($\phi z+$) and pronation ($\phi z-$).

Motion was expressed by three translations (Δx, Δy, Δz) along and three rotations (ϕa, ϕb, ϕc) about the axes of the radial coordinate system. The measured motion was interpolated for every 5° of wrist motion between 50° extension and 80° flexion, and between 40° ulnar deviation and 40° radial deviation. Additionally, the total translation ($\Delta_{tot} = \sqrt{(\Delta x)^2 + (\Delta y)^2 + (\Delta z)^2}$) and total rotation ($\varphi_{tot} = \sqrt{(\Delta\varphi_x)^2 + (\Delta\varphi_y)^2 + (\Delta\varphi_2)^2}$) were calculated as proposed by Kuo et al., (2014).

To investigate if the position of the fracture line with respect to the scaphoid apex influences the relative motion of the scaphoid fragments, we quantified motion between the distal and proximal scaphoid fragments, and compared motion parameters in these two fracture-line categories. Subsequently, we investigated if uncoupling between the distal carpal row (represented by the capitate), proximal carpal row (represented by the lunate) and the lever (scaphoid) exists in case of a scaphoid nonunion, by comparing motion patterns of bones in the affected wrist with those of the healthy contralateral wrist. To this end we quantified and evaluated: (1) relative motion between the distal carpal row (capitate) and the proximal carpal row (lunate), (2) if the scaphoid nonunion fragments follow the proximal carpal row (lunate) to assess the influence of the scapholunate ligament, (3) how the scaphoid fragments move with respect to the radius, to allow comparison with other studies.

Identifying the fracture location and quantification of the scaphoid nonunion flexion deformity

To identify the scaphoid nonunion fracture location, the mirrored contralateral healthy scaphoid was proximally aligned with the proximal pole of the affected scaphoid. The scaphoid apex was manually determined in 3-D from the healthy scaphoid. The apex is a non-articulating part of the scaphoid, located at the most ulnar point on the dorsal ridge (Figure 1). The fracture line in the affected scaphoid was subsequently classified as starting distal or proximal from the apex. Second, the degree of distal fragment collapse was expressed in terms of an anatomical coordinate system of the scaphoid, by subsequently aligning the distal segment with the healthy scaphoid reference (Figure 4). Fragment collapse was expressed in one total translation (Δ_{tot}) and one total rotation parameter (ϕ_{tot}). Results are presented in Table 1.

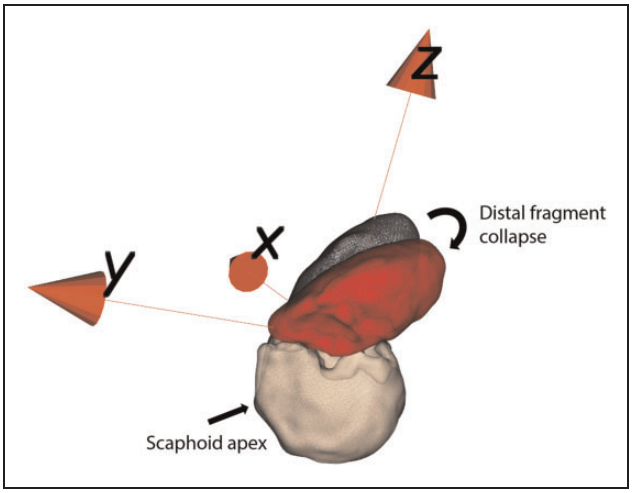

Figure 4. Scaphoid nonunion with a fracture line distal to the scaphoid apex. The grey mesh represents the contralateral healthy scaphoid of the patient. The proximal fragment (bone colour) is aligned with the proximal pole of the healthy scaphoid. Subsequently the distal pole (red) is aligned with the healthy reference to quantify the collapse. Fragment displacement is calculated in 3-D. Automatic coordinate system placement is based on the axes of inertia of the healthy scaphoid.

Statistical methods

To analyse the influence of fracture location on fragment instability, the patients were divided in two groups: patients with the fracture line distal and proximal to the apex. For both FE and RUD motion, a linear mixed-effects model was used to determine the association of fracture location to fragment instability. Participants were included as a random factor; the 6° of freedom (Δx, Δy, Δz, ϕa, ϕb, ϕc), total translation (Δ_{tot}) and total rotation (ϕ_{tot}) as dependent factors; and wrist motion and fracture location as fixed factors. Additional mixed models were used to evaluate if the presence of DISI, duration of nonunion, wrist movement and scaphoid nonunion flexion deformity were associated with increased fragment instability. *P*-values were obtained by likelihood ratio tests using analysis of variance (ANOVA) of the full model with the effect in question, against the model without the effect in question (Bolker et al., 2009). To evaluate if DISI deformity significantly influenced the amount of fragment collapse, a paired Student's *t*-test was used.

To evaluate if carpal uncoupling occurred after nonunion, multiple linear mixed effect models were used. The motion patterns of the healthy wrists were compared with the wrists with the scaphoid nonunion. Different models were built to evaluate if the presence of a nonunion is associated with a different motion

pattern. We separately evaluated the relative motion of the scaphoid to the radius; of the scaphoid to the lunate; and of the capitate to the lunate. Again, a likelihood ratio test using ANOVA was used to compare the models. To evaluate if the range of motion of the wrist (defined as the rotation of the capitate relative to the radius) was significantly altered after a scaphoid nonunion, a paired Student's *t*-test was used.

Results

Seven patients with a fracture line proximal and five patients with a fracture line distal relative to the apex of the scaphoid were included in this study. The location of the fracture line was not associated with an increase of interfragmentary motion between the scaphoid fragments for FE and RUD wrist motion (Supplementary Table S1, Supplementary Figure S1A, S1B). Increased interfragmentary motion was significantly correlated with the presence of DISI for ϕ_{tot} ($\chi 2$ (1) = 5.1, $p = 0.02$*), resulting in a 5° (SD 2°) increase of total fragment rotation during FE wrist motion (Figure 5, Supplementary Figure S2). DISI deformity significantly influenced the amount of fragment collapse ($p = 0.007$, 95% CI −21 to −5). Patients with a DISI had a mean distal fragment collapse of 31° (SD 6°), while in patients with no DISI deformity the mean fragment collapse was 18° (SD 7°). Increased fragment instability was correlated with the duration of nonunion (FE: Δ_{tot} $p = 0.02$*; RUD, Δ_{tot} $p = 0.002$*), wrist movement (FE: Δx, Δy, Δz, ϕa, ϕb, ϕc, Δ_{tot}; all $p < 0.001$* and RUD: Δx, Δy, Δz, ϕa; all $p < 0.01$*) and scaphoid nonunion flexion deformity (FE: Δx $p = 0.04$*, ϕa $p = 0.04$*)

The second part of this research evaluated if a scaphoid nonunion results in an uncoupling of the distal and proximal carpal rows. A scaphoid nonunion significantly affected capitolunate motion during wrist FE and RUD motion (Figure 6, Supplementary Table S2, Supplementary Figure S3A, S3B). In healthy wrists, the capitate moved 54° (SD 12°) in relation to the lunate, this relative motion changed significantly in wrists with a scaphoid nonunion, in which the capitate moved only 40° (SD 13°) relative to the lunate ($p = 0.015$*, 95% confidence intervals (CI): 3 to 24).

For the global motion of the scaphoid relative to the radius, the proximal fragment translated in a reversed motion pattern compared with the motion pattern of a healthy scaphoid (Figure 7, Supplementary Figure S4A, S4B), during wrist FE and RUD motion. This reversed translation of the proximal pole was also observed in the motion relative to the lunate (Figure 7, Supplementary Figure S5A, S5B). Results of all statistical tests are presented in Supplementary Tables S3 and S4.

The range of motion of the wrist was significantly decreased for all patients after a scaphoid nonunion. Healthy wrists had a mean FE of 104° (SD 13°) and wrists with a nonunion a mean of 83° (SD 17°) ($p < 0.01$*; 95% CI: 8 to 33). The mean range of RUD motion was 56° (SD 8°) for healthy wrists and 47° (SD 10°) for nonunion wrists ($p < 0.05$*; 95% CI: 1 to 17).

Discussion

Our study showed no association of scaphoid fracture location to increased scaphoid fragment instability. However, we did find that increased fragment instability predominantly depends on the presence of a DISI deformity. Interestingly, this is similar to the results described by Moritomo et al. (2008), since all of their patients in the 'mobile group' were described as having a DISI deformity, and all of the patients in the 'stable group' did not have a DISI deformity. Since our patient population consisted of patients with a proximal fracture line with/without DISI deformity, and patients with a distal fracture line with/without DISI deformity, we could differentiate between the effects of the fracture location and the effect of a DISI deformity on fragment instability. Therefore, our trial concludes that it is not the fracture location, but a DISI deformity which results in increased scaphoid nonunion fragment instability. The influence of the fracture location on fragment instability was also evaluated by Leventhal et al. (2008). In their six patients with a scaphoid nonunion, five had a distal fracture line and one a proximal fracture line relative to the apex. They found that fracture location was not associated with increased fragment instability. In their population four patients had a DISI deformity. Unfortunately, they did not evaluate the effect of DISI on fragment instability.

We found that a scaphoid nonunion results in a complete uncoupling of the proximal and distal carpal row, with adapted motion patterns in the distal carpal row (represented by the capitate), the proximal carpal row (represented by the lunate) and in the lever (scaphoid). A scaphoid nonunion affected the surrounding carpal bones and significantly influenced the relative motion between the capitate and lunate (Figure 6, Supplementary Table S2). With a DISI deformity present, the relative capitolunate motion reduces from 54° to 40°. It is expected that a DISI deformity would result in less relative motion. However, we also found that the motion profile of the capitolunate motion changes significantly when a scaphoid nonunion is present (Figure 6).

Additionally, the proximal scaphoid translated in an almost reversed motion pattern compared with the healthy contralateral scaphoid (Figure 7) in relation

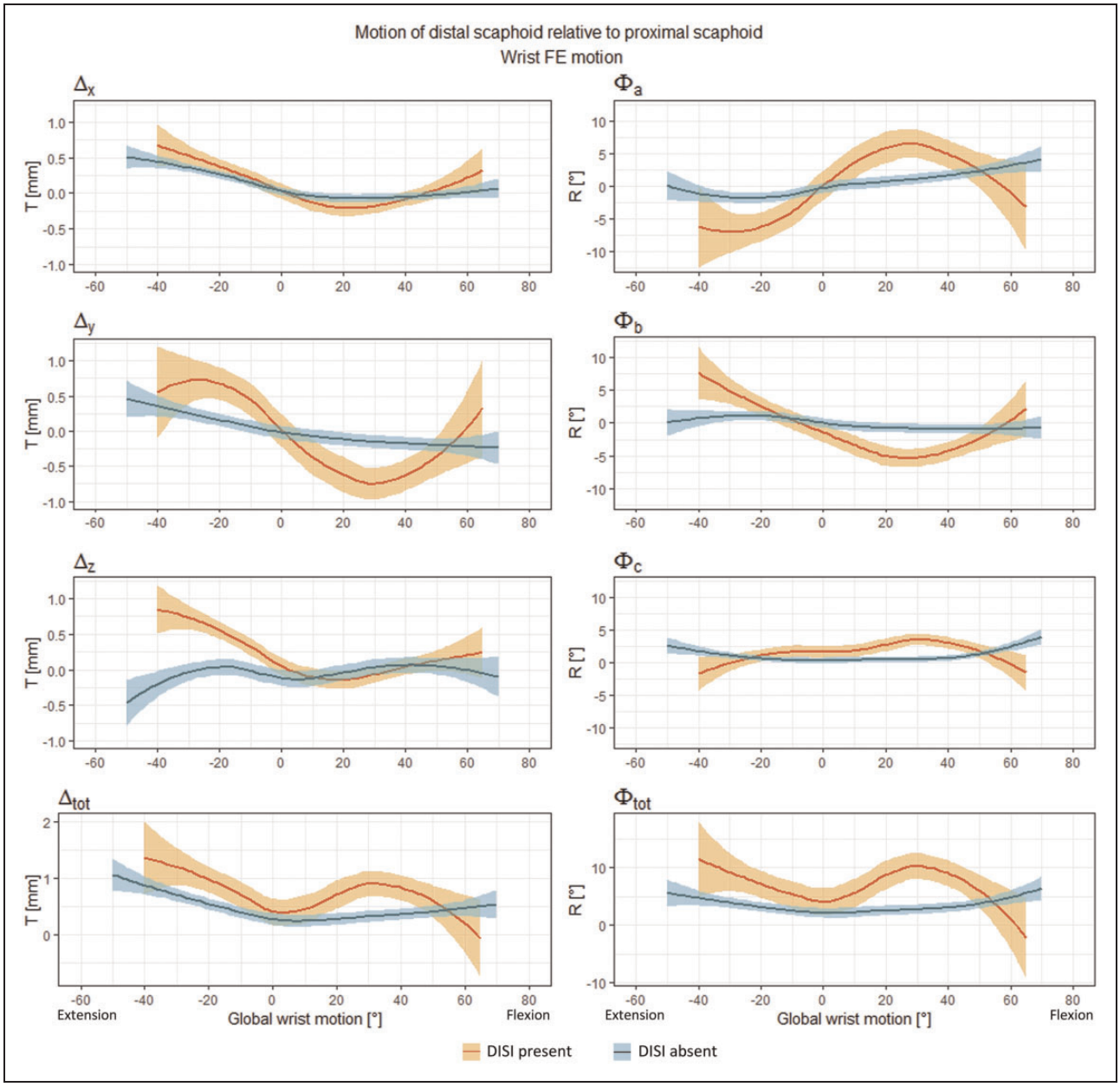

Figure 5. Motion of the distal scaphoid relative to the proximal scaphoid during flexion–extension of the wrist. Increased fragment instability is correlated with the presence of a DISI deformity.
T: translation; R: rotation.

to the radius, which was also described by Leventhal et al. (2008). The motion of the scaphoid nonunion fragment relative to the lunate was evaluated. Movement of the proximal scaphoid fragment was significantly different from the healthy contralateral scaphoid relative to the lunate. We did not expect this finding, due to the close relationship between the lunate, proximal pole of the scaphoid and scapholunate ligament. Additionally, we found that the distal scaphoid fragment demonstrated a normal scaphoid motion pattern in relation to the lunate.

Identifying which factors cause a wrist to develop a DISI deformity, and thus carpal collapse after a scaphoid non-union, remain unanswered. Research has been done on the influence of lunate morphology on the development of a DISI deformity in patients with scaphoid nonunion (Haase et al., 2007; Kim et al., 2016), with a type I lunate being associated with a higher incidence of DISI deformity. In our patient population three patients with a lunate type I and two patients with a lunate type II presented with a DISI deformity. However, the size of our patient population

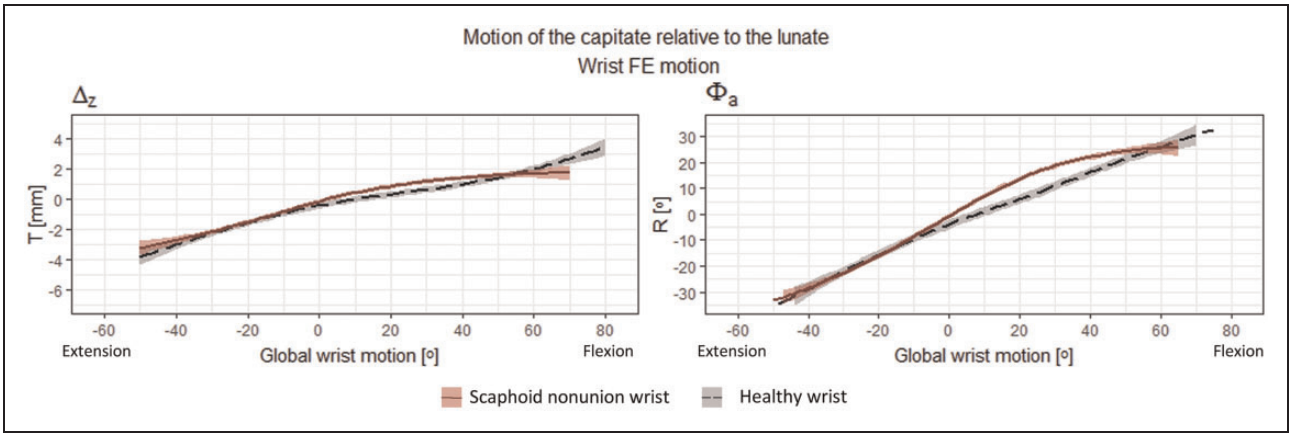

Figure 6. Motion of the capitate relative to the lunate. During wrist flexion, the relative capitatolunate motion alters compared to the healthy wrist.
T: translation; R: rotation.

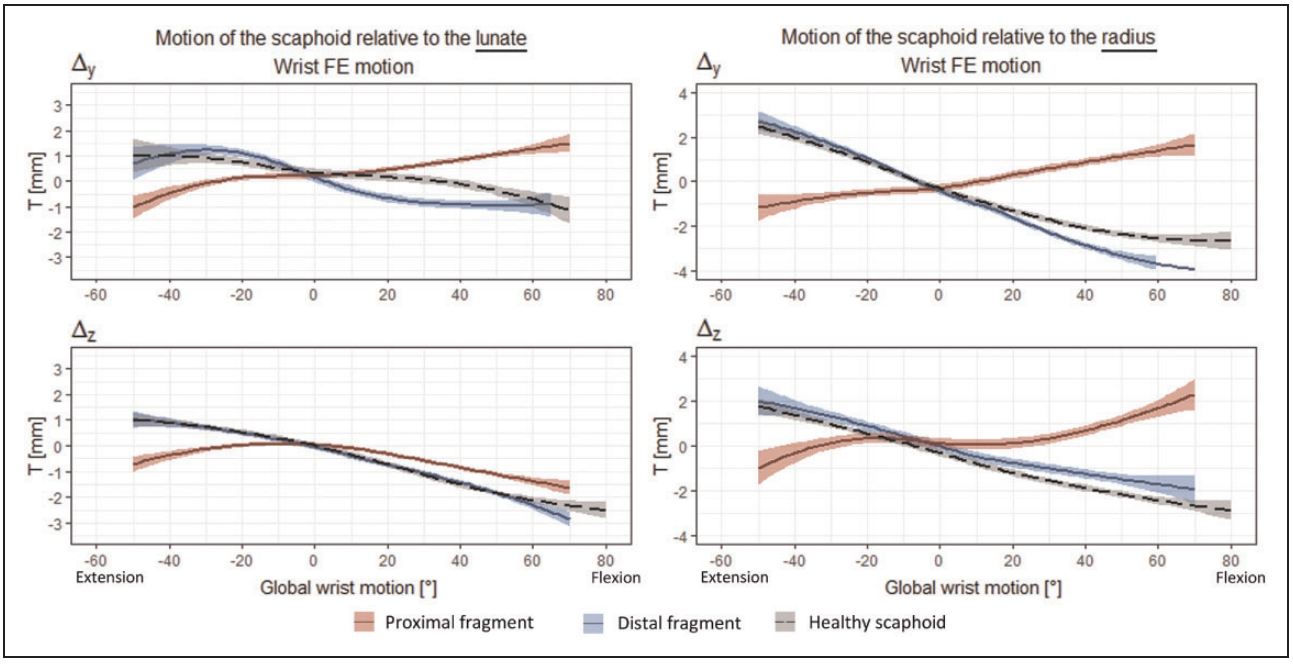

Figure 7. Motion of the scaphoid fragments and healthy scaphoid relative to the lunate and radius. The proximal scaphoid fragment translates in a reversed motion pattern, compared with the healthy scaphoid motion pattern.
T: translation.

was too small to draw conclusions on the influence of lunate morphology on the occurrence of DISI.

As expected, analysing carpal kinematics with 4-D-CT imaging provided additional insights in the adapted motion patterns after scaphoid nonunion compared with only analysing carpal alignment at extreme wrist positions. As seen in Figures 5 and 7, the largest position changes in carpal alignment were not at extreme wrist positions. Additionally, due to measurements of every 5° of wrist motion, we could identify the point at which the pathological carpal motion pattern starts to alter from normal kinematics. This can be seen in Figure 6, in which the relative capitatolunate motion pattern only starts to deviate during wrist flexion, but eventually joins the normal kinematic reference line again during extreme wrist flexion.

One of the limitations of this study is the small number of patients with a unilateral scaphoid nonunion, thus far-reaching conclusions cannot be made. However, with the studies of Moritomo et al. (2008) and Leventhal et al. (2008) combined, we could compare the motion patterns of 31 scaphoid nonunion cases, in which our study was the first to

evaluate the full range of motion with 4-D-CT imaging. We decided not to evaluate the dart-throwing motion pattern of the wrist, because previous studies demonstrated that proximal carpal row motion is minimized during a dart-throwing motion and motion predominantly occurs in the midcarpal joint (Crisco et al., 2005; Werner et al., 2004, 2016b).

In conclusion, we found that increased instability of the scaphoid fragments is associated with the presence of a DISI deformity of the carpus, and is not dependent on the position of the fracture line relative to the scaphoid apex. A scaphoid nonunion results in an uncoupling of the proximal and distal carpal rows, which significantly influences the motion patterns of surrounding carpal bones.

Acknowledgement We would like to thank J. van Lieshout, plastic surgeon, for including patients in the OLVG hospital, location Oost.

Declaration of conflicting interests The authors declared no potential conflicts of interest with respect to the research, authorship, and/or publication of this article.

Funding The authors received no financial support for the research, authorship, and/or publication of this article.

Ethical approval Data collection was approved by the Medical Ethics Committee of the Academic Medical Center, University of Amsterdam, Amsterdam. With reference number: NL56112.018.15.

Supplemental material Supplemental material for this article is available online.

References

Adolfsson L, Povlsen B. Arthroscopic findings in wrists with severe post-traumatic pain despite normal standard radiographs. J Hand Surg Br. 2004, 29: 208–13.

Bolker BM, Brooks ME, Clark CJ et al. Generalized linear mixed models: a practical guide for ecology and evolution. Trends Ecol Evol. 2009, 24: 127–35.

Citteur JM, Ritt MJ, Bos KE. Carpal boss: destabilization of the third carpometacarpal joint after a wedge excision. J Hand Surg Br. 1998, 23: 76–8.

Crisco JJ, Coburn JC, Moore DC, Akelman E, Weiss AP, Wolfe SW. In vivo radiocarpal kinematics and the dart thrower's motion. J Bone Joint Surg Am. 2005, 87: 2729–40.

de Lange A, Kauer JM, Huiskes R. Kinematic behavior of the human wrist joint: a roentgen-stereophotogrammetric analysis. J Orthop Res. 1985, 3: 56–64.

Dobbe JGG, de Roo MGA, Visschers JC, Strackee SD, Streekstra GJ. Evaluation of a quantitative method for carpal motion analysis using clinical 3D and 4D CT protocols. IEEE Trans Med Imaging. 2019, 38: 1048–57.

Ferguson DO, Shanbhag V, Hedley H, Reichert I, Lipscombe S, Davis TR. Scaphoid fracture non-union: a systematic review of surgical treatment using bone graft. J Hand Surg Eur. 2016, 41: 492–500.

Haase SC, Berger RA, Shin AY. Association between lunate morphology and carpal collapse patterns in scaphoid nonunions. J Hand Surg Am. 2007, 32: 1009–12.

Kuo HY, Su HR, Lai SH, et al. 3D object detection and pose estimatino from depth image for robotic bin picking. IEEE International Conference on Automation Science and Engineering (CASE), Taipei. 2014: 1264–9.

Kim BJ, Kovacevic D, Lee YM, Seol JH, Kim MS. The role of lunate morphology on scapholunate instability and fracture location in patients treated for scaphoid nonunion. Clin Orthop Surg. 2016, 8: 175–80.

Leventhal EL, Wolfe SW, Moore DC, Akelman E, Weiss AP, Crisco JJ. Interfragmentary motion in patients with scaphoid nonunion. J Hand Surg Am. 2008, 33: 1108–15.

Mack GR, Bosse MJ, Gelberman RH, Yu E. The natural history of scaphoid non-union. J Bone Joint Surg Am. 1984, 66: 504–9.

Miric D, Karovic B, Senohradski K. [Role of wrist instability in the onset of pseudoarthrosis of the scaphoid bone]. Srp Arh Celok Lek. 2000, 128: 384–8.

Moritomo H, Murase T, Oka K, Tanaka H, Yoshikawa H, Sugamoto K. Relationship between the fracture location and the kinematic pattern in scaphoid nonunion. J Hand Surg Am. 2008, 33: 1459–68.

Moritomo H, Tada K, Yoshida T, Masatomi T. The relationship between the site of nonunion of the scaphoid and scaphoid nonunion advanced collapse (SNAC). J Bone Joint Surg Br. 1999, 81: 871–6.

Moritomo H, Viegas SF, Elder KW et al. Scaphoid nonunions: a 3-dimensional analysis of patterns of deformity. J Hand Surg Am. 2000, 25: 520–8.

Oka K, Moritomo H, Murase T, Goto A, Sugamoto K, Yoshikawa H. Patterns of carpal deformity in scaphoid nonunion: a 3-dimensional and quantitative analysis. J Hand Surg Am. 2005, 30: 1136–44.

Rainbow MJ, Kamal RN, Leventhal E et al. In vivo kinematics of the scaphoid, lunate, capitate, and third metacarpal in extreme wrist flexion and extension. J Hand Surg Am. 2013, 38: 278–88.

Slutsky DJ. The incidence of dorsal radiocarpal ligament tears in patients having diagnostic wrist arthroscopy for wrist pain. J Hand Surg Am. 2008, 33: 332–4.

Tatebe M, Hirata H, Tanaka K, Oguchi T, Urata S. Scaphoid nonunion with carpal ligament injury – radiological, arthroscopical assessment and clinical results. Acta Orthop Belg. 2016, 82: 210–5.

von Elm E, Altman DG, Egger M et al. The strengthening the reporting of observational studies in epidemiology (strobe) statement: guidelines for reporting observational studies. Int J Surg. 2014, 12: 1495–9.

Vroemen JC, Dobbe JG, Jonges R, Strackee SD, Streekstra GJ. Three-dimensional assessment of bilateral symmetry of the radius and ulna for planning corrective surgeries. J Hand Surg Am. 2012, 37: 982–8.

Werner FW, Green JK, Short WH, Masaoka S. Scaphoid and lunate motion during a wrist dart throw motion. J Hand Surg Am. 2004, 29: 418–22.

Werner FW, St-Amand H, Moritomo H, Sutton LG, Short WH. The effect of scaphoid fracture site on scaphoid instability patterns. J Wrist Surg. 2016a, 5: 47–51.

Werner FW, Sutton LG, Basu N, Short WH, Moritomo H, St-Amand H. Scaphoid tuberosity excursion is minimized during a dart-throwing motion: a biomechanical study. J Hand Ther. 2016b, 29: 175–82.

Wong TC, Yip TH, Wu WC. Carpal ligament injuries with acute scaphoid fractures – a combined wrist injury. J Hand Surg Br. 2005, 30: 415–8.